ISBN: 978-3-95450-230-1 ISSN: 2673-5350 doi:10.18429/JACoW-IBIC2021-TUPP15

4D BEAM TOMOGRAPHY AT THE UCLA PEGASUS LABORATORY

V. Guo*, P. Denham, P. Musumeci, A. Ody, and Y. Park,
UCLA Department of Physics and Astronomy, Los Angeles, CA, USA

Abstract

We present an algorithm to tomographically reconstruct the 4D phase space of a beam distribution of a high brightness electron beam, based on the use of two fluorescent screens separated by a beamline containing a quadrupole triplet which can be used to impart arbitrary rotations to the beam phase space. The reconstruction method is based on generating a macroparticle distribution which matches the initial profile and then it is iteratively updated using the beam projections on the second screen until convergence is achieved. This process is repeated for many quadrupole current settings. The algorithm is benchmarked against GPT simulations, and then implemented at the UCLA Pegasus beamline to measure the phase space distribution for an upcoming high speed electron microscope experiment.

INTRODUCTION

In high brightness electron accelerators, the beam dynamics and transport is strongly influenced by the space charge fields associated with the details of the electronic distribution and its evolution along the beamline, which depends on each particle position and velocity [1]. In linear beam dynamics, it is sufficient to monitor the second order moments of the distribution which has a constant shape along the beamline, but as soon as non-linear forces (either external or internal) are applied, the distribution will evolve and change along the beamline. Having an accurate representation of the beam transverse phase space is then critical to predict and then optimize the beam behavior in many setups. For example in single-shot time-resolved electron microscopy, it has been pointed out that different electronic distribution can originate different space-charge induced aberrations and greatly affect the spatial resolution of the instrument [2].

While it is of great interest to know the shape of the transverse phase space distribution function, the experimental measurement of this quantity poses some challenges as beam profile monitors only record the spatial beam distribution (i.e. the projection of the 4D phase space volume onto the x-y plane) while the angular or transverse velocity distribution is harder to access.

Tomography is a well developed imaging technique that uses a set of projections to reconstruct a distribution in a space with higher dimensions. Typically, tomography is used to reconstruct the shape of an object in 3D from a complete set of 2D projections along different angles as for example in CAT scans. Applied to beam physics, tomography can be used to reconstruct the 4D phase space distribution from an appropriately chosen set 2D transverse beam profile (projections) [3–6].

* vgwr618@g.ucla.edu

In this paper, we present the development of such a technique at the UCLA Pegasus Laboratory [7, 8] where fluorescent screens are used to record the spatial projections of a high brightness beams before and after a set of three quadrupoles with adjustable currents to change the rotation angles of the transverse phase space and enable a tomographic reconstruction. Importantly, the transformation of the phase space in these measurements does not provide projections for the entire range of rotation angles due to the limitation in the quadrupole currents or placement of the beamline components. Therefore, while usual tomography reconstructs the source volume from complete set of projections over the entire range of possible angles [9, 10], the algorithm for beam phase space reconstruction should be tolerant of this incomplete set of projections. We present here the MATLAB algorithm we used in the reconstruction which is based on sampling the 4D beam transverse phase space with a macroparticle distribution. The algorithm is shown to work well both on simulation and experimental data and is eventually expected to be used in a feedback loop to optimize the photocathode illumination to generate ideally shaped 4D transverse phase space distributions to improve spatial resolution in single shot time-resolved electron microscopy.

DATA COLLECTION

In order to perform a tomographic reconstruction, sufficient access to different rotation angles is needed. While the technique can be generalized and applied to other beamlines, in the following we focus on the setup currently installed at the UCLA Pegasus laboratory shown in Fig. 1. The measurement takes place in the area highlighted by the red square. The initial spatial distribution is recorded on screen 4 and the various projections are obtained changing the currents in the green quadrupoles with the beam profile recorded on the final YAG screen.

The current settings for the quadrupoles are chosen in order to maximize the range of angles the phase space rotates before hitting the final screen.

In order to do this, we write the beam transport matrix as a function of current settings on each of the quadrupole (I_1, I_2, I_3) using a smooth approximation for the quadrupole field gradient profile $G(z)$ along the axis:

$$G(I,z) = \frac{CI}{2}\left[\tanh\left(\frac{b}{2}\left(\frac{L}{2}-z\right)\right)+\tanh\left(\frac{b}{2}\left(\frac{L}{2}+z\right)\right)\right]$$

where L is the effective length of the quadrupole, b is the steepness parameter of the edges, and the nominal magnetic field gradient CI is simply proportional to the current setting of the quadrupole. For the quadrupoles used in the experiment $L = 0.078\,\mathrm{m}$, $b = 135\,\mathrm{m}^{-1}$ and $C = 0.45\,\mathrm{Tm}^{-1}\mathrm{A}^{-1}$.

ISBN: 978-3-95450-230-1 ISSN: 2673-5350 doi:10.18429/JACoW-IBIC2021-TUPP15

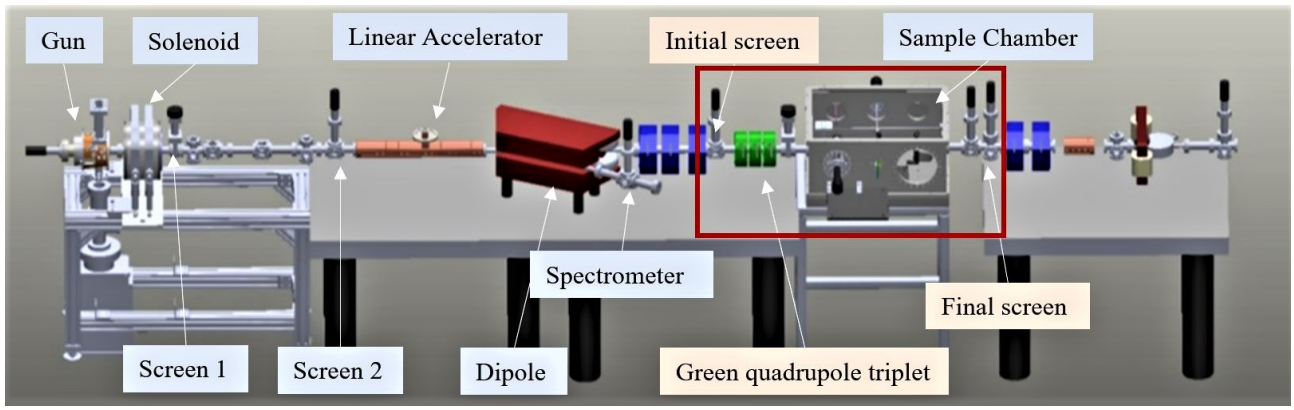

Figure 1: Schematic of the UCLA Pegasus beamline. Initial screen projection is collected at screen 4. The green quadrupole triplets perform rotations on the beam. Spatial projection images after rotation are collected at the final screen. The red box shows where the experiment takes place.

The overall gradient function for our beamline can be obtained by the superposition of $G_I(z)$ for each quadrupole. The locations of the screens and the quadrupoles along the beamline are given in Table 1.

Table 1: Locations of the Screens and the Quadrupoles Along the UCLA Pegasus Beamline

Beamline Component	Position
Screen 4	3.191 m
Green Quadrupole 4	3.295 m
Green Quadrupole 5	3.381 m
Green Quadrupole 6	3.466 m
Final Screen	4.500 m

The matrix transport is checked to match the General Particle Tracer (GPT) simulation of the beam envelope evolution as shown in Fig. 2.

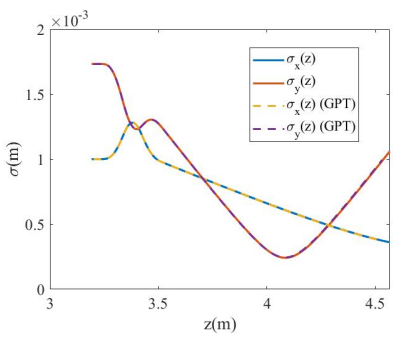

Figure 2: The envelope evolution of a Gaussian beam under quadrupole current settings 1.41 A, -2.39 A, and 1.17 A. The dashed lines shows the evolution under GPT simulation and the solid lines shows the evolution using the step transport matrices.

For uncoupled transport, the 2D transport matrix can also be defined by affine transformation $M = SER$, where S, E, and R are the shear, expansion, and rotation matrix respectively:

$$M = \begin{pmatrix} 1 & 0 \\ k & 1 \end{pmatrix} \begin{pmatrix} e_1 & 0 \\ 0 & \frac{1}{e_1} \end{pmatrix} \begin{pmatrix} \cos(\theta) & -\sin(\theta) \\ \sin(\theta) & \cos(\theta) \end{pmatrix}.$$

We can then obtain the overall rotation angles θ_x and θ_y from the beam transport matrix,

$$\theta_x = \arccos\left(\frac{M_{1,1}}{\sqrt{M_{1,1}^2 + M_{1,2}^2}}\right), \; \theta_y = \arccos\left(\frac{M_{3,3}}{\sqrt{M_{3,3}^2 + M_{3,4}^2}}\right),$$

which is dependent on the current settings. Setting goal x- and y- rotations from 0 to π, the desired quadrupole current settings can be computed using a nonlinear least square optimization. The obtained current settings are used to collect final screen images under different rotations.

Accessible angles are limited to the middle of the rotation space due to the quadrupole and screen positions as well as the current setting limits. In addition the final screen has a diameter of 8 mm which also poses a limit on the available rotation angles. The rotation angles used in the simulations and experiments discussed below are shown in Fig. 3.

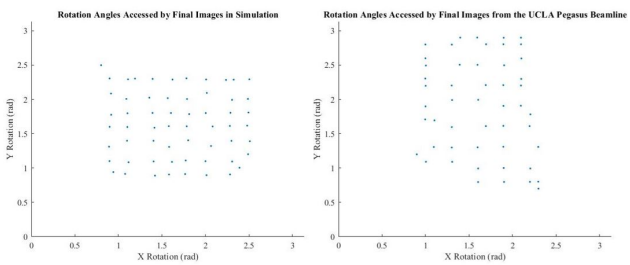

Figure 3: On the left is the x- and y- rotation angles of each set of quadrupole settings used in simulation. On the right is the x- and y- rotation angles of each set of quadrupole settings used in the Pegasus beamline experiment.

ISBN: 978-3-95450-230-1 ISSN: 2673-5350 doi:10.18429/JACoW-IBIC2021-TUPP15

RECONSTRUCTION ALGORITHM

To reconstruct the 4D transverse phase space (x, x', y, y'), we developed an algorithm that starts from the spatial projection as measured by screen 4 and attempts to match the projections on the final screen resulting after applying rotations using three quadrupoles.

We begin by initializing a number N of macroparticles using the image at the initial screen as the probability distribution for the x-y coordinates. A random uniform momentum distribution is then assigned to the ensemble, which gives us an initial guess 4D distribution (x_i, x_i', y_i, y_i').

For each set of quadrupole settings, the guess ensemble is transported to the final screen using the beam transport matrix. The phase space distribution so obtained is then projected onto the $x - y$ plane and then compared with the data image at the final screen. Particles that landed in pixels having excess charge compared to the measured image are marked as candidates to be respawned. After the marking process is repeated through all the quadrupole settings in the data sets, particles that failed to land in the correct pixels for more than k images are respawned with values from a 4D normal distribution centered at 0 with standard deviation from the second-order moment matrix of the particles that survived the marking process. The algorithm terminates when the number of particles that need to be respawned is less than p% of the total number of macroparticles used. The convergence parameters k and p can be altered based on need for precision.

Reconstruction of Simulation

To test the reconstruction algorithm, we generated a test data set using GPT formed by an initial screen image and 59 final screen images with different quadrupole current settings. The algorithm then reconstructs the test distribution using those images.

The test beam we chose is Gaussian in its spatial distribution with a double Gaussian momentum distribution. This choice is made to demonstrate the algorithm's ability to converge towards a momentum space with a complicated inner pattern. The distribution to be reconstructed is shown in Fig. 4.

Setting the convergence parameters to be $k = 1$ and $p = 1$, the algorithm was able to reconstruct the full 4D phase space in 7.46 s on a standard personal laptop using four cores. The momentum reassignment loop stopped after 22 iterations when the particles that landed in an over-dense region in more than one image is less than 1% of the total number of particles used.

While the reconstructed phase space shown in Fig. 5 can give a good idea of the ability of the algorithm to reconstruct the initial distribution we can also compare the second order moment matrix which is found to agree within 10% of the initial beam matrix.

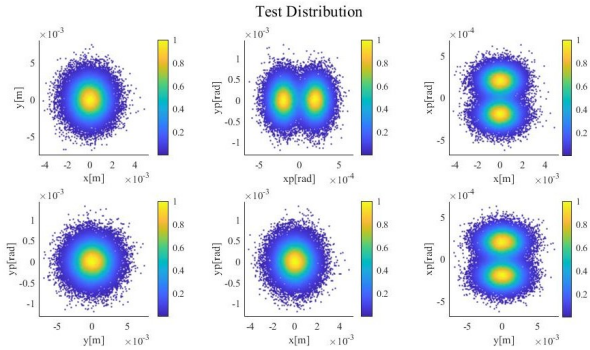

Figure 4: Simulated test distribution to be reconstructed.

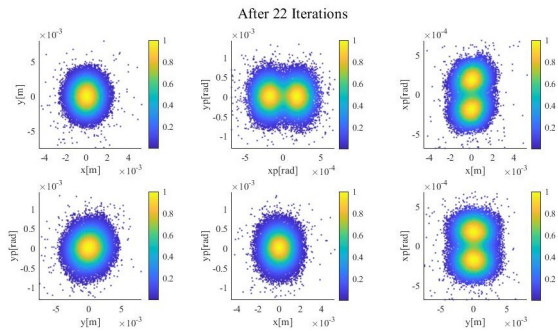

Figure 5: The reconstructed 4D phase space after 22 iterations of momentum reassignment.

Reconstruction of Experimental Data

The algorithm was then used on experimental data collected from the UCLA Pegasus laboratory. The beam energy for these measurements was 8.7 MeV and the beam charge was 2 pC. An initial screen image was taken at screen 4 and used as a probabilistic intensity mask to obtain the initial spatial distribution as shown in Fig. 7. A guess Gaussian momentum distribution with $\sigma_x = 4 \times 10^{-4}$ rad and $\sigma_y = 3 \times 10^{-4}$ rad is initialized with this spatial distribution to create a guess initial 4D distribution. The number of macroparticles used to simulate the distribution is 50,000.

The initial 4D distribution is then transported to the final screen position using the beam transport matrices based on each set of quadrupole current settings and compared against 50 data images from the beamline. Setting the algorithm hyper-parameters to be $k = 5$ and $p = 15$, the runtime is 361.78 s using four cores on a personal laptop. Figure 6 shows the comparison between the data images and the reconstructed phase space projections. The point-spread function used in the displayed trial is 18.63 µm. In order to take into account for the Poissonian statistics associated with the limited number of macroparticles used to sample the beam distribution, the noise parameter from image filtering is set as 0.5 so that a particle will be marked to be respawned if $p_r - p_t > 0.5 \cdot \sqrt{p_t}$ where p_r is the count value of the pixel the particle lands in and p_t is the corresponding value from the same pixel in the target data image. The reconstructed

ISBN: 978-3-95450-230-1 ISSN: 2673-5350 doi:10.18429/JACoW-IBIC2021-TUPP15

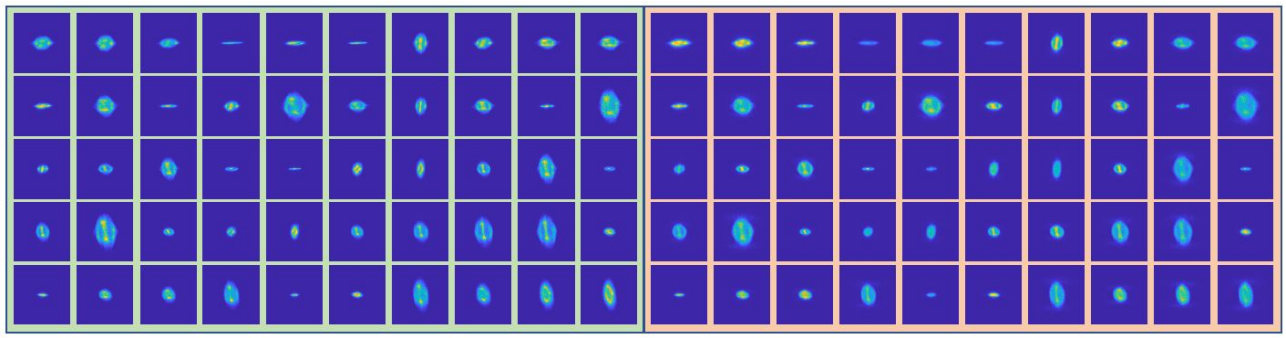

Figure 6: The left box contains 50 final images from the UCLA Pegasus beamline. The right box are the corresponding final images based on the reconstructed 4D phase space.

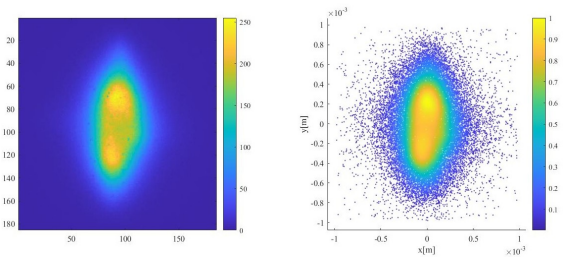

Figure 7: The left shows the initial screen 4 image collected from the UCLA Pegasus beamline. The right shows the spatial distribution the algorithm initializes based on the screen image.

distribution has a beam geometric emittance of 41 nm. The distribution is shown in Fig. 8.

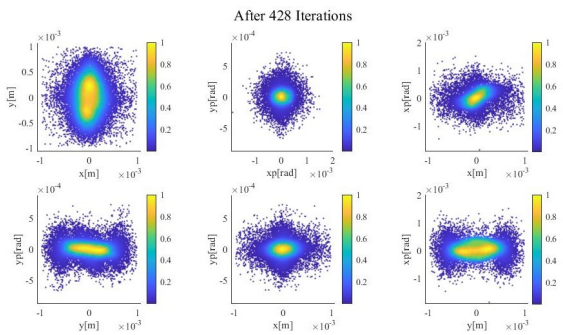

Figure 8: The reconstructed 4D phase space after 428 iterations of momentum reassignment.

In comparison with the simulation case, reconstruction using experimental data is much more difficult due to noise and image quality. The reconstruction time increases with the number of images used. Additionally, tighter parameter control–i.e. allowing smaller number of images to be missed, stopping at lower number of particles to be respawned, or decreasing the noise parameter–can all result in a longer reconstruction time.

CONCLUSION

We have presented a method to tomographically reconstruct the full 4D transverse phase space distribution. The method uses one initial screen projection, three quadrupoles for beam rotation, and a final screen for spatial projections of the beam's final distribution. Sufficient access to the rotation angles in both x and y is needed in order to get an accurate reconstruction. Using an iterative momentum reassignment algorithm, the method can reconstruct the full 4D phase space with reasonable computational time. We have verified the algorithm by applying it to a simulated distribution. Using collected images from GPT, the algorithm was able to reconstruct complicated inner patterns within the momentum space. The reconstructed distribution closely matches the original distribution.

The algorithm is tested on data images collected from the UCLA Pegasus beamline. Although the reconstruction time is higher than in simulation, the algorithm is able to reconstruct a 4D transverse phase space that produces images that well match the final spatial projections of the actual beam under 50 quadrupole-controlled rotations. Potential future improvements that could be made include understanding the role of the space charge fields in the measurements, decreasing the reconstruction time, optimizing image processing method to reduce noise, and improving reconstruction accuracy.

ACKNOWLEDGMENTS

This work has been supported by the National Science Foundation under Grant No. PHY-1549132 and grant PHY-1734215 and DOE grant No. DE-SC0009914. PD was supported by National Science Foundation under Grant No. DMR-1548924.

REFERENCES

[1] P. Musumeci, J. G. Navarro, J. Rosenzweig, L. Cultrera, I. Bazarov, J. Maxson, S. Karkare, and H. Padmore, "Advances in bright electron sources," *Nuclear Instruments and Methods in Physics Research Section A: Accelerators, Spectrometers, Detectors and Associated Equipment*, vol. 907, pp. 209–220, 2018.

ISBN: 978-3-95450-230-1 ISSN: 2673-5350 doi:10.18429/JACoW-IBIC2021-TUPP15

[2] P. Denham and P. Musumeci, "Space-charge aberrations in single-shot time-resolved transmission electron microscopy," *Physical Review Applied*, vol. 15, no. 2, p. 024050, 2021.

[3] B. Hermann, V. A. Guzenko, O. R. Hürzeler, A. Kirchner, G. L. Orlandi, E. Prat, and R. Ischebeck, "Electron beam transverse phase space tomography using nanofabricated wire scanners with submicrometer resolution," *Physical Review Accelerators and Beams*, vol. 24, no. 2, p. 022802, 2021.

[4] F. Hannon, I. Bazarov, B. Dunham, Y. Li, and X. Liu, "Phase Space Tomography Using the Cornell ERL DC Gun", in *Proc. 11th European Particle Accelerator Conf. (EPAC'08)*, Genoa, Italy, Jun. 2008, paper TUPC032, pp. 1119–1121.

[5] K. Hock, M. Ibison, D. Holder, A. Wolski, and B. Muratori, "Beam tomography in transverse normalised phase space," *Nuclear Instruments and Methods in Physics Research Section A: Accelerators, Spectrometers, Detectors and Associated Equipment*, vol. 642, no. 1, pp. 36–44, 2011.

[6] D. Xiang, Y.-C. Du, L.-X. Yan, R.-K. Li, W.-H. Huang, C.-X. Tang, and Y.-Z. Lin, "Transverse phase space tomography using a solenoid applied to a thermal emittance measurement," *Physical Review Special Topics-Accelerators and Beams*, vol. 12, no. 2, p. 022801, 2009.

[7] D. Alesini, A. Battisti, M. Ferrario, L. Foggetta, V. Lollo, L. Ficcadenti, V. Pettinacci, S. Custodio, E. Pirez, P. Musumeci, *et al.*, "New technology based on clamping for high gradient radio frequency photogun," *Physical Review Special Topics-Accelerators and Beams*, vol. 18, no. 9, p. 092001, 2015.

[8] J. Maxson, D. Cesar, G. Calmasini, A. Ody, P. Musumeci, and D. Alesini, "Direct measurement of sub-10 fs relativistic electron beams with ultralow emittance," *Physical Review Letters*, vol. 118, no. 15, p. 154802, 2017.

[9] V. Yakimenko, M. Babzien, I. Ben-Zvi, R. Malone, and X.-J. Wang, "Electron beam phase-space measurement using a high-precision tomography technique," *Physical Review Special Topics-Accelerators and Beams*, vol. 6, no. 12, p. 122801, 2003.

[10] C. McKee, P. O'Shea, and J. Madey, "Phase space tomography of relativistic electron beams," *Nuclear Instruments and Methods in Physics Research Section A: Accelerators, Spectrometers, Detectors and Associated Equipment*, vol. 358, no. 1-3, pp. 264–267, 1995.